EFDA–JET–PR(08)29

Y. Corre, E. Joffrin, P. Monier-Garbet, Y. Andrew, G. Arnoux, M. Beurskens, S. Brezinsek, M. Brix, R. Buttery, I. Coffey, K. Crombe, E.de La Luna, R. Felton, C. Giroud, S. Hacquin, J. Hobirk, A. Huber, F. Imbeaux, S. Jachmich, M. Kempenaars, X. Litaudon, H. Leggate, T. Loarer, G. Maddison, E. Rachlew, J. Rapp, O. Sauter, A. Savchkov, G. Telesca, A. Widdowson, K.D. Zastrow, O. Zimmermann and JET-EFDA collaborators

Hybrid H-Mode Scenario with Nitrogen Seeding and Type III ELMs in JET

Hybrid H-Mode Scenario with Nitrogen Seeding and Type III ELMs in JET

Y. Corre[1], E. Joffrin[1], P. Monier-Garbet[1], Y. Andrew[2], G. Arnoux[1], M. Beurskens[2], S. Brezinsek[3], M. Brix[2], R. Buttery[2], I. Coffey[4], K. Crombe[5], E.de La Luna[6], R. Felton[2], C. Giroud[2], S. Hacquin[1], J. Hobirk[7], A. Huber[3], F. Imbeaux[1], S. Jachmich[8], M. Kempenaars[2], X. Litaudon[1], H. Leggate[2], T. Loarer[1], G. Maddison[2], E. Rachlew[9], J. Rapp[3,10], O. Sauter[11], A. Savchkov[2], G. Telesca[3], A. Widdowson[3], K.D. Zastrow[2], O. Zimmermann[3] and JET-EFDA collaborators[*]*

JET-EFDA, Culham Science Centre, OX14 3DB, Abingdon, UK

[1]CEA, IRFM, F-13108 Saint-Paul-lez-Durance, France.
[2]EURATOM-UKAEA Fusion Association, Culham Science Centre, OX14 3DB, Abingdon, OXON, UK
[3]Institut für Energieforschung - Plasmaphysik, Forschungszentrum Jülich, Association EURATOM-FZJ Trilateral Euregio Cluster, Germany
[4]Queen's University, Belfast, BT7 1NN, UK
[5]Department of Applied Physics, Ghent University, Rozier 44, B-9000 Ghent, Belgium
[6]EURATOM–CIEMAT, Laboratorio National de Fusion. Spain
[7]Max-Planck Institut fuer Plasmaphysik, EURATOM Association, Garching, Germany
[8]Association EURATOM-Belgian State, KMS-ERM B-1000, Brussels, Belgium
[9]Association EURATOM-VR, KTH Roy. Inst. of Tech., SE-10691 Stockholm, Sweden
[10]FOM Instituut voor Plasmafysica Rijnhuizen, EURATOM Association, Trilateral Euregio Cluster, Nieuwegein, The Netherlands.
[11]Association EURATOM Confédération Suisse, CRPP - EPFL, 1015 Lausanne, Switzerland
** See annex of M.L. Watkins et al, "Overview of JET Results ", (Proc. 21 st IAEA Fusion Energy Conference, Chengdu, China (2006)).*

Preprint of Paper to be submitted for publication in
Plasma Physics and Controlled Fusion

ABSTRACT.

The performance of the 'hybrid' H-mode regime (long pulse operation with high neutron fluency) has been extensively investigated in JET during the 2005-2007 experimental campaign up to normalized pressure $\beta_N = 3$, toroidal magnetic field $B_t = 1.7$T, with type I ELMs plasma edge conditions. The optimized external current drive sources, self-generated non-inductive bootstrap current and plasma core stability properties provide a good prospect of achieving a high fusion gain at reduced plasma current for long durations in ITER.

One of the remaining issues is the erosion of the divertor target plates associated with the type I ELM regime. A possible solution could be to operate with a plasma edge in the type III ELM regime (reduced transient and stationary heat loads) obtained with impurity seeding. An integrated hybrid type III ELM regime with a normalized pressure $\beta_N = 2.6$ ($P_{NBI} \sim$ 20-22MW) and a thermal confinement factor of $H^*_{98}(y,2) \sim 0.83$ has been recently successfully developed on JET with nitrogen seeding. This scenario shows good plasma edge condition (compatible with the future ITER-like wall on JET) and moderate MHD activity. In this paper, we report on the experimental development of the scenario (with plasma current $I_p = 1.7$MA and magnetic field $B_t = 1.7$T) and the trade-off between heat load reduction at the target plates and global confinement due to nitrogen seeding and type III ELM working conditions.

1. INTRODUCTION

The reference H-mode scenario (H for high confinement) for ITER [1], is expected to meet the goal of fusion gain $Q = 10$ at $\beta_N = 1.8$ for a few hundred seconds. To increase discharge duration in ITER with sufficient fusion gain ($Q > 5$), it is necessary to maximize the self-generated non-inductive current fraction by decreasing the plasma current and increasing the plasma pressure. Higher pressure could generate pressure driven plasma instability such as the neo-classical tearing modes NTMs that are often triggered by sawtooth collapse. In this context, the so-called 'hybrid' scenario has successfully eliminated the deleterious effect of sawteeth activity by establishing a broad current density profile in stationary state with safety factor q close to unity in the plasma core. Originally operated in ASDEX Upgrade [2] and DIII-D [3], extended in JET [4], this scenario provides a promising route to ITER operation with reduced flux consumption and high neutron fluence [5]. Similarly to the standard H-mode, two of the remaining issues of the 'hybrid' scenario for long pulse operation with the type I ELM regime are that of first wall material erosion (which limits the lifetime of Plasma Facing Components - PFC) and of heat loads which can lead to unacceptable damage of PFCs (melting, sublimation, cracks, boiling of the water in the cooling pipes and ultimately water leaks).

Due to the problem of Tritium (T) retention in carbon PFCs, the materials presently envisaged in ITER are Beryllium (Be) in the main chamber, tungsten (W) in the divertor baffle region and Carbon (C) for a restricted number of targets (at the location with highest heat load) to minimize T-retention in the vessel. To test ITER-relevant plasma scenarios in the JET tokamak, it is planned to

install a beryllium first wall and apply a tungsten coating [6] on the full set of tiles in the divertor (ITER-like wall project [7]). In ITER (actively cooled device), but also on JET with the future ITER-like wall (inertial cooling device), low erosion rates and sustainable heat loads (transient and stationary) will be necessary to preserve the integrity of the machines. In order to prepare the operation of 'hybrid' discharges with the ITER-like wall in JET and long 'hybrid' discharges in ITER, we have investigated the capability of impurity seeding to reduce the heat loads and the feasibility to operate the 'hybrid' scenario with type III ELM [8] (where both transient and stationary heat loads mitigation are possible in contrast to type I ELM regime where only stationary heat load mitigation has been achieved [9]).

During ELMy H-mode operation, when external gas fuelling is applied, the ELM frequency increases while the energy confinement is reduced, further increase of the gas fuelling usually leads to the transition from type I to type III ELM [10]. Type III ELM are likely to be caused by resistive ballooning instabilities [11], thus favorably at high plasma collisionality ($n^*_e = Z_{eff} n_e qR/T_e^2$). According to a wide experimental study dedicated to the standard H-mode scenario on JET, it turns out that at the transition from type I to type III ELM, the pedestal temperature (and pressure) always drop off whether the pedestal density increases or decreases [12]. Impurity seeding is used in our experiment to modify the edge plasma parameter in that sense (reduced pedestal temperature). Nitrogen impurity is chosen here because of its high radiating efficiency at low plasma temperature. In JET attached plasmas, nitrogen (ionization potential of $E_i = 15.58$eV) is expected to radiate mainly in the divertor near the X-point and upstream of the divertor targets. Impurity seeding has initially been applied to standard H-mode discharges to achieve type III ELMs. After successful application [8], impurity seeding is extended to 'hybrid' H-mode regime initially performed with type I ELMs (with plasma current $I_p = 1.7$MA and toroidal magnetic field $B_t = 1.7$T). One of the main issues of such an experiment was to establish if the hybrid scenario (characterised here by the MHD stability rather than the energy confinement) could be sustained with type III ELMy H-mode in the plasma edge. In the reference 'hybrid' regime, the maximum radiated power fraction achieved with deuterium fuelling alone is P^{rad}/P^{tot}~35% (mainly C plus substantial D radiation). An additional nitrogen injection brings the radiated fraction up to 50% (mainly C plus N radiation). This corresponds to the type III ELM regime (obtained here when the pedestal temperature $T^{ped} \leq 750$ eV and $P^{rad}/P^{tot}>40\%$.).

The set-up and the description of the hybrid scenario with impurity seeding are presented in chapter 2. The plasma modifications due to N seeding are discussed separately during the type I ELM regime (chapter 3) and type III ELM regime (chapter 4). A comparison between D and N injection is also proposed in chapter 3 in order to balance the advantages and disadvantages regarding heat loads and plasma confinement. Analysis of the plasma characteristics (radiation, temperature, density and heat loads) into the pedestal region, near the X-point, into the scrape-off layer and near the target plates respectively, is presented. A net reduction of the transient (during ELM) and stationary (inter-ELM) heat loads on the divertor tiles is achieved during the type III ELM regime at the expense of the plasma energy confinement. The trade-off between heat load reduction and plasma

performance degradation due to impurity seeding is discussed in chapter 5 and conclusions are drawn in chapter 6.

2. DESCRIPTION OF THE HYBRID H-MODE SCENARIO WITH IMPURITY SEEDING.

2.1. HYBRID SCENARIO EXPERIMENTAL SET-UP

The target plasma scenario is a hybrid H-mode (defined here as an optimized scenario for high b_N operation with moderate MHD activity) with type-I ELMs (Pulse No: 68505), where pedestal plasma temperature is $T^{ped} \sim 1000$eV, plasma current $I_p = 1.7$MA, toroidal magnetic field $B_t = 1.7$T, central density $\langle n_e \rangle \sim 5\times10^{19}$ m^{-3} (~ 70% of the Greenwald density), edge safety factor $q_{95} \sim 3.2$ in which injected neutral beam power (NBI) is feed-back controlled to ~14-16MW to achieve a total normalized pressure of $\beta_N = 3$. The thermal confinement enhancement factor achieved in the target plasma scenario is $H^*_{98}(y,2) \sim 1.05$ and the plasma effective charge is $Z_{eff} \sim 1.8$. A high triangularity magnetic configuration ($\delta = 0.44$) is used with full carbon MkII-HD divertor (with Load-Bearing Septum Replacement Plate LBSRP as shown in figure 1). Lower hybrid heating is used during the plasma current ramp up (for a duration of ~ 3s) to delay the plasma current profile penetration with the aim of producing a broad q profile when the main heating is applied. This is followed by an intermediate $\beta_N = 2$ phase (for a duration of ~ 3s) for stabilization of the q-profile close to 1 in order to minimize the impact of sawtooth on stability. The β_N request is then increased and kept constant during 4 seconds. During this phase, a pre-set injection of deuterium is applied: $\beta_N \sim 3$ has been obtained with low deuterium fuelling (hybrid reference no 1 Pulse No: 68505: $\Phi_D = 0.6\times10^{22}$ electrons per second) and $\beta_N = 2.6$ with high deuterium fuelling and density close to the Greenwald density $n_e \sim 0.95 \bullet n_{Gr}$ (hybrid reference no 2 Pulse No: 68515, 68738: $F_D = 5\times10^{22}$ e/s).

2.2. SEEDING TECHNIQUE ON THE SCENARIO

Nitrogen injection is applied in addition to deuterium fuelling during the first three seconds of the high β_N plateau (when $\beta_N = 2.6$). Deuterium is injected in the bottom of the divertor near the outer strike point on the Low Field Side (LFS) while nitrogen is injected into the private-flux region from the horizontal target plate located on the High Field Side (HFS), as shown in figure 1.

The experimental scenario and timing are presented in figure 2 with pre-programmed nitrogen injection (preset fuelling rate). A real-time control feed-back technique can also be applied to control the radiated power (measured with the bolometric system) with the nitrogen injection during the high-b_N plateau. The feed-back controller includes the filtering of the radiation fraction and uses both integral and derivative gains as described in [13]. The real-time control feed-back is an efficient tool to find the quantity of gas needed to reach high radiative fraction and thus find the transition from type-I to type-III ELM regime.

2.3. OPERATIONAL DOMAIN COVERED DURING THE EXPERIMENT

The maximum radiated power fraction achieved with deuterium fuelling alone (with mainly D and

C radiators) is P^{rad}/P^{tot}~37% with density close to the Greenwald limit $n_e \sim n_{Gr}$ (Pulse No: 68739). Figure 3a shows the limit of the radiated fraction achieved with deuterium fuelling alone (when the density approaches the Greenwald limit, the fuelling rate increases exponentially while the radiated fraction stay quasi-constant). Using deuterium plus nitrogen fuelling enables to increase the radiative fraction (with mainly D, C and N radiators), ~50% has been achieved during the experiment (#68532 in figure 3a). These values have been determined by using an average of the bolometer signal (sampling rate of 2 ms) during the *inter-ELM period*. Since the radiation *during ELMs* is higher (peaks of radiation) this corresponds basically to the baseline of the bolometer time trace. The type III ELM regime, characterized by high ELM frequency (~500Hz) and small amplitude (visible and IR transient peaks are reduced), is achieved here when $P^{rad}/P^{tot} > 40\%$ and the pedestal ion temperature T^{ped} is below 750eV. Figures 3a (fuelling and radiation) and 3b (pedestal temperature and density) summarized the operational domain achieved to develop the hybrid type III ELM regime in JET (including pre-programmed and feed-back seeding discharges). A particular and intermediate regime characterized by the occurrence of compounds ELMs (i.e. mixed type I/type III ELMs separated by brief ELM free periods) is obtained for high pedestal densities, when approaching the type III ELM plasma conditions (as shown in figure 3b). The distinction between the compounds ELM regime with the standard type I ELM regime is sometimes very narrow and thus difficult to establish correctly without any optimized diagnostic set-up and power variation (traditionally used to make the distinction). Discharges including compounds ELMs are reported in figure 3b within the dashed circle.

Figure 4 shows some of the main plasma parameters for the hybrid type III ELM regime (Pulse No: 68532 obtained with both radiative and b_N real-time control) compared to the reference hybrid type I ELM regime with high D-fuelling (Pulse No: 68515 obtained with β_N real-time control only). In the seeded-discharge, the strong initial gas puff ($\Phi_D = 5\times10^{22}$ e/s and $\Phi_N \sim 7\times10^{22}$ e/s) decreases the pedestal temperature (from ~1000eV to ~700eV) and produces the transition to the type III ELM regime.

Before the transition phase, i.e. during the type-I ELM regime (when $P^{rad}/P^{tot} < 40\%$ and $T^{ped} >$ 750eV), a significant leakage of the seeded impurity out of the divertor is observed, as also reported in [14]. Once the pedestal temperature is reduced and the type-III ELM is obtained, the impurity gas puff needed to maintain constant radiated power and therefore the regime stationary is decreasing slowly from $\Phi_N \sim 6\times10^{22}$ down to $\Phi_N \sim 3\times10^{22}$ e/s. The total radiated power fraction achieved with the type III ELM regime is ~ 50% with $\beta_N = 2.6$ (P_{NBI} ~ 20-22 MW) and the thermal confinement enhancement factor is $H^*_{98}(y,2) \sim 0.83$ (Pulse No: 68532), about 20% less than the reference type I ELM discharge (Pulse No: 68505). The confinement loss is due to the pedestal energy degradation and the residual MHD activity (see next section). The positive effect associated to the type III ELM regime is a net reduction of the heat load on the divertor tiles that are normally subject to high heat flux (discussed in details in chapter 4). Also discussed in chapter 4 is the nitrogen impurity concentration responsible for the relatively high Z_{eff} observed in the hybrid type III ELM (figure 4d). Before N-seeding (t < 8s), the difference in Z_{eff} is due to release of the trapped nitrogen from

preceding discharges to Pulse No: 68532. During N-seeding (t = 8-11 s), Z_{eff} increases and stabilized around 3. The plasma modification due to N_2 injection in the type I ELM regime is discussed separately in chapter 3.

2.4. MHD AND PLASMA STABILITY

The MHD activity is characterized by mild n=1 sawteeth precursors present during the high β_N phase (visible by the burst in the magnetic spectrogram depicted in figure 5b), suggesting that the minimum safety factor q_{min} is equal to or smaller than 1 (as confirmed with the motional Stark effect measurement presented in figure 5a). During the hybrid type-III ELM, an n=3 mode (destabilized at t = 6s before the impurity seeding is applied, i.e. when $\beta_N = 2$) is present near the q = 4/3 surface, as described in [15]. The more deleterious 2/1 and 3/2 NTM are not present during the hybrid type-III ELM case and nor in the reference type-I case. The residual MHD island (4/3 NTM) is about 3cm wide and explains only partially the confinement degradation observed during the type-III ELM regime (compared to the type-I ELM case in which the 4/3 NTM is not present): the loss of confinement associated to the 4/3 NTM is estimated to be $\delta H = 4 \cdot (\text{width}/a) \cdot (r_{4/3}/a)^3$, $\approx 5\%$ where a is the minor plasma radius and $r_{4/3}$ is the radial position of the q = 4/3 magnetic surface [16].

3. PLASMA MODIFICATION DUE TO D AND N FUELLING DURING THE HYBRID TYPE I ELM REGIME

3.1. EFFECT OF FUELLING ON PEDESTAL

To assess separately the effect of D fuelling and N seeding on the plasma edge characteristics, a series of D and N pre-programmed fuelling scans have been performed in the reference hybrid type I ELM scenario. The D and N fuelling values designed for the scans are reported in number of electrons per second (e/s). The D fuelling scan is spanning from low to high electron fuelling rates $\Phi_D = (0.6\text{-}9)\times10^{22}$ e/s (the D_2 influx is equivalent to the number of electron injected per second divided by the atomic number N = 2), corresponding to the following series of Pulse No's: 68505, 68515, 68516 and 68739 (see table 1). The highest value of the D fuelling rate scheduled in the experiment was limited by the energy confinement drop (the thermal confinement factor measured during Pulse No: 68739 is $H^*_{98}(y,2) \sim 0.82$) and because P^{rad}/P^{tot} does not increase anymore (as shown in figure 3a). The N fuelling scan is limited to low electron fuelling rates in the $\Phi_N = (0.6\text{-}2.1)\times10^{22}$ e/s range (the N_2 influx is obtained by dividing the electron flux by the charge factor Z = 7 and the atomic number N=2), this corresponds to the following series of Pulse No's: 68505, 68507, 68508, 68509 and 68510 (see table 1). The highest value of the N fuelling rate scheduled in the experiment was limited by the need to keep the effective charge of the plasma below a value of $Z_{eff} \sim 3$. The modification of the plasma ion temperature (measured by the edge CXRS diagnostic [17]) due to D and N fuelling is presented in figure 6.

Increasing deuterium fuelling reduces the ion temperature at the top of the pedestal from 1000 eV to below 800 eV while the electron density at the pedestal is varying from $\langle n_e^{ped} \rangle \sim 4\times10^{19} m^{-3}$

to ~ 5.5×10^{19} m^{-3} and the radiated fraction is increasing from P^{rad}/P^{tot} ~ 25% to ~ 35%. On the other hand, at low plasma density and with the limited level of N fuelling rates used in the experiment, increasing nitrogen fuelling does not increase the radiation significantly and consequently does not influence the plasma ion temperatures (circles in figure 6a) while Z_{eff} is varying from ~ 1.8 (Pulse No: 68505) to ~ 2.7 (Pulse No: 68510, value that sets a limit on the N injection when the D fuelling is low). The cooling effect observed in the pedestal region with D injection is coherent with the increase of density and radiated power (also correlated to the occurrence of compound ELMs), as shown in figure 6b (P^{rad} increases from 4.5MW to 7.5MW). The experimental strategy used to develop the hybrid type-III ELM scenario is to cool the pedestal with deuterium and nitrogen injection in order to optimize, simultaneously, the radiation efficiency (to access to the type-III ELM regime) and Z_{eff}.

3.2. EFFECT OF FUELLING ON HEAT LOAD

The effect of D and N fuelling on the heat load is different of that observed on the ion temperature. It has been established in [9] that transient heat load in the type-I ELM regime is only marginally affected by impurity radiation (ELM mitigation with impurity seeding does not appear to be an efficient tool in JET ELMy H-mode plasmas). In this section (dedicated to the type-I ELM regime), we focus therefore our interest on the stationary heat load. The modification of the deposited heat load due to N and D fuelling has been studied using two independent diagnostics, namely a set of thermocouples embedded into the divertor tiles (this system is very reliable and not perturbed by any carbon surface layer effect; but it measures only the bulk temperature) and the IR wide angle viewing system that measures the surface temperature [18].

The energy distribution in the divertor integrated allover the discharge, derived from the ThermoCouple (TC) measurement, shows a significant reduction in tiles No 5 and 6 (where the outer strike point is located, as shown in figure 1; and where the inter-ELM heat load is maximal) when N fuelling rate is increased. The total energy loaded into the outer tile N∞6 during the pulse is ~ 25MJ without and ~ 20MJ with N seeding, while it remains constant when increasing the deuterium fuelling rate. This effect is even more visible when looking directly at the thermocouples data during the plateau when the fuelling is applied. As a first approximation, the heat load averaged over transient and stationary phases can be qualitatively estimated by looking at the difference of temperature DT_{TC} (in degree) between the *end* and the *beginning* of the seeded phase, measured by one of the embedded TC (at 1 cm from the surface of the tile). Note that this qualitative estimation of Q does not depend on any carbon surface layer on the top of the tile (while it is sometimes problematic for the interpretation of the IR data). In figure 7 we plot the difference of temperature DT_{TC} measured in tile No 6 (near the Outer Strike Point – OSP) divided by the total input power in order to study the variation of the heat load (mainly made up of the conducted power near the OSP) when N and D fuelling is applied. On contrast to D injection alone that is completely inefficient to mitigate the surface temperature, N injection results systematically (i.e. independently of the pre-set deuterium fuelling rate – see N scans in figure 7) in lower DT_{TC}/P^{tot}, which implies lower heat

loads. This effect is not completely understood and requires further investigations. In the low radiated fraction region (when f^{rad} inter-ELM is < 35%), the averaged heat load reduction obtained with N injection is about a factor of 2 ($\Delta T_{TC}/P^{tot}$~2.7°/MW obtained with $F_N{}^3$). In the high radiated fraction region (when f^{rad} inter-ELM is > 35%), the maximum temperature reduction obtained with nitrogen ($\Delta T_{TC}/P^{tot}$~1.2°/MW for $F_N{}^3$) compared to deuterium ($\Delta T_{TC}/P^{tot}$~3.7°/MW in average) injection is a factor of 3 near the OSP.

The benefit of N injection to reduce the heat loads is confirmed by the averaged (over transient and stationary phases during the seeding phase) peak heat flux estimated from the IR wide angle viewing system [18]. On the outer strike point (tile No 6) the peak heat flux (maximum of the heat flux distribution computed along the surface of the poloidal cross section of the tiles with the 2D non-linear code THEODOR [19]) is reduced by almost a factor of two (therefore consistent with TC data presented above): from $\langle Q_{target}^{OSP} \rangle = 1.7 MW\, m^{-2}$ with D fuelling only (reference pulse Pulse No: 68505) to $\langle Q_{target}^{OSP} \rangle = 1.7 MW\, m^{-2}$ with N fuelling (Pulse No: 68510; $\Phi_N{}^3 = 2.2\times10^{22}$ e/s). This is also observed during similar experiment using impurity seeding in Advance Tokamak scenario with Internal Transport Barrier (ITB) recently developed at JET [20, 21]. N-seeding alone enables to mitigate the energy and power load during the stationary phase keeping quasi-constant the pedestal temperature profile. To reduce the ELM energy, it is necessary to reach higher radiative power fraction and hence, get a degraded edge pedestal as reported in [22].

4. PLASMA MODIFICATION OBSERVED DURING THE HYBRID TYPE III ELM REGIME WITH N_2 SEEDING

4.1. EDGE PEDESTAL

The reference hybrid scenario with low D-fuelling (Pulse No: 68505: $\Phi_D = 0.6\times10^{22}$ e/s) shows a pedestal ion temperature of ~1000eV (measured at the top of the pedestal with the edge CXRS diagnostic [17] – figure 8). A slightly higher temperature is observed for the electron with the core and edge LIDAR Thomson scattering measurements [23] (figure 9a).

Such plasma conditions are associated with type-I ELM behavior with high peak heat flux (up to ~60 MW m^{-2} as reported in JET [24, 20]) leading to high erosion rates during ELMs. As discussed in the previous chapter, increasing deuterium fuelling (Pulse No: 68515: $\Phi_D = 5\times10^{22}$ e/s) reduces the pedestal ion temperature below 800eV. The radiated fraction does not increase significantly (maximum f^{rad} reached with D-fuelling is ~37%, see figure 3a, and the averaged ELM frequency stays around 50-65Hz, see table1) and the type-III ELMs regime is not achieved. For higher level of D injection ($\Phi_D = 5\times10^{22}$ e/s) adding N-seeding leads to simultaneous increase of the radiated fraction up to 50%, while the pedestal ion temperature drops below 750eV (figure 8a) and the type-III ELM regime is triggered.

The edge plasma modifications (in the pedestal region) due to D- fuelling type-I ELM and N-fuelling type-III ELM are also illustrated in figure 9. In addition to the observed cooling of the ions in the pedestal region, the temperature gradients are different with and without N-seeding. The

electron temperature gradient (figure 9a) is outboard shifted (by about 3cm) when N_2 is seeded while the electron density gradient does not move (figure 9b). This modification is not yet explained. Because of possible change shot to shot in the laser beam alignment of the edge LIDAR Thomson scattering diagnostic (leading to probable high uncertainties on the radial position), optimized edge plasma measurements (using for example the newly installed JET High Resolution Thomson Scattering system [25] that produces high spatial resolution profiles of n_e, T_e and p_e) will be necessary to better characterize and validate such behavior.

4.2. PLASMA RADIATION

As presented in figure 10a, the modification of the plasma radiation due to N seeding is illustrated by the horizontal bolometer camera measurements taken during the inter-ELM phase (viewed from the bottom to the top of the machine). Thomographic reconstructions of P_{rad} derived from the horizontal and vertical bolometer cameras are presented in figure 10b and 10c. The divertor radiation is increased by almost a factor of two near the X-point (bolometer channel No 3 as indicated in figure 10a) and by about a factor of three (300%) just inside the separatrix (bolometer channel n∞4), traducing an increase of the radiated volume. The radiated power into the divertor region is estimated to be $P_{rad}^{div} \sim 4$MW without (Pulse No: 68515) and $P_{rad}^{div} \sim 7$MW with N seeding (Pulse No: 68532).

In addition, the signals measured by the lines of sight passing through the core (channel n∞5 to 20) are increased by almost a factor of two in average. This is consistent with the total bulk radiation that is estimated to be $P_{rad}^{bulk} \sim 2$MW without and $P_{rad}^{bulk} \sim 4$MW with type-III ELM obtained with N seeding. The relatively high bulk radiation is due to the impurity contamination, as suggested by the increase of Z_{eff} (shown in figure 4) and the nitrogen core concentration that is measured with the core CXRS diagnostic: $N^{7+}/n_e \sim 2\%$ (data shown latter on, in figure 16). The volume of plasma mostly affected by the nitrogen radiation is near the X point, preferably inside the separatrix as also illustrated in figures 10b and 10c.

4.3. HEAT LOAD ON TARGETS

The heat load reduction associated with the type-III ELM regime is illustrated in figure 11 (IR data with sampling rate of 6 ms) and figure 12 (TC data with sampling rate of 50ms). The amplitude of the surface temperature measured with the wide-angle thermographic viewing system [18], shows a net reduction during the N-seeding phase from t = 8 to 11s (during transient and stationary phases of the discharge). During the *inter-ELM periods*, when the plasma is in quasi-stationary condition after the ELM collapse, the surface temperature remains stable (T^{surf} is controlled) on the outer target plate where the heat flux is expected to be maximum (blue curve in figure 11c). *During ELMs*, the IR sampling rate is not optimized to measure the true surface temperature (especially during the type-III ELM regime where $\langle f_{ELM} \rangle \sim 500$ Hz). The surface temperature variation DT_{ELM} measured during ELMs can be used anyway, in first approximation, to study their amplitude. Figure 11 shows that DT_{ELM} is almost completely mitigated ($\langle \Delta T_{ELM} \rangle \sim 10^o$) on the upper dump plate and

outer limiter, and *partially* reduced ($<\Delta T_{ELM}> \geq 200^{o}$ during the type-I and ~ 100^{o} during the type-III ELM regime) on the outer target plate region. Optimized IR data (with higher frame rate and reduce image size, up to 10kHz is achievable with the JET wide-angle thermographic system [26]) are necessary to quantify the ELM mitigation effect. Simultaneously, the bulk temperature is stabilized on the outer target plate where the heat flux is normally higher with forward magnetic field [27] (T^{bulk} is controlled, thus reinforcing the previous IR statement).

The total energy load on the outer tile No 6 overall the pulse is 15MJ with the hybrid type-III ELM scenario and 25 MJ during the reference hybrid type-I ELM scenario (figure 12). The time-averaged (over transient and stationary phases during the seeding phase) peak heat flux computed on the outer strike point (with the 2D non-linear code THEODOR [19]) during the type-III ELM hybrid regime is $\langle Q_{target}^{OSP} \rangle = 0.4 MW\, m^{-2}$, corresponding to a net peak heat load reduction in both the ELM and inter-ELM periods of about a factor 4 compared to the reference hybrid type-I ELM regime (where $\langle Q_{target}^{OSP} \rangle = 1.7 MW\, m^{-2}$).

4.4. EROSION ON TARGETS

In addition to the Deuterium (D) fuelling, the Nitrogen (N) seeding in the divertor can also modify the plasma wall interaction and sputtering processes, that play a role in the erosion rate of the target plates and consequently in the PFC lifetime (a critical issue for the divertor target plate in ITER). The modification of molecular (CD and CN band) and carbon (CII line) emissions in the divertor due to the N fuelling is observed with two spectrometers (labelled KT3A/B) monitoring the Outer Strike Point (OSP) region with a good spectral and spatial resolution (12.5mm) [28, 29]. The first spectrometer (KT3A) monitors the divertor targets in the near UV wavelength range (λ = 384–398 nm) and allows the detection of CN, CII and NII emission (fig.13). The second spectrometer (KT3B) monitors the same region in the visible wavelength range (λ = 426-429nm) and allows the detection of CD and CII emission. The time evolution of the released species due to N-seeding is depicted in figure 14, showing a significant reduction of CD Gerö band ($A^2\Delta \rightarrow X^2\Pi$) and CII line emission during N-seeding.

This can be explained in part by a reduction of the plasma density near the OSP, as measured by the Langmuir probe: $\langle n_e^{edge} \rangle \sim 10^{19}\, m^{-3}$ during the reference hybrid pulse and $<n_e^{edge}> \sim 2\times10^{18}\, m^{-3}$ during the hybrid type-III ELM pulse (suggesting a possible partial plasma detachment) while the edge plasma temperature stays constant[1] ($<T_e^{edge}>$ lies between 5 and 10eV near the OSP during both the reference and the type-III ELM hybrid regimes). Since no measurements precisely localized at the OSP are available, it is not clear whether a cooling effect is produced on the target or not. The variation of plasma density modifies directly the line emission efficiency (proportional to the electronic density) but also indirectly (through the incident particle flux) the sputtering processes and thus the carbon sources. In the meantime, the CN molecule emission becomes higher (see the averaged spectrum over the seeding phase in figure 13) indicating an increase of the chemical processes involving nitrogen and carbon. Further investigations relying on particle flux and erosion

[1] *Note that the Langmuir probe used in this section is not located exactly on the OSP but a little bite further away in the direction of the private flux region.*

yield calculation (the procedure is described in [30]) are required to determine which one of the following factors is responsible for the global reduction of CII: the "density" effect alone or with an additional "cooling" effect (leading to a lower sputtering yield), or the "chemical" effect (due to a possible film suppression and a particular low erosion rate in presence of active species such as N_2 [31]). New plasma experiments with the OSP localized precisely on the Langmuir probe and quartz micro balance data with at least 5 second exposure time (to get ride of the noise) to monitor the film growth or suppression [32] would be required.

5. INTEGRATED HYBRID TYPE III ELM PERFORMANCE

The hybrid type III ELM scenario obtained by N-seeding has been successfully developed in JET with $I_p = 1.7$MA, $q_{95} \sim 3.2$, $n_e \sim 0.95 \cdot n_{Gr}$ and total $\beta_N \sim 2.6$. The plasma performance of this scenario is illustrated in figure 15, which represents the global energy confinement factor $H98_{(y,2)}$ as a function of the radiated fraction for a series of hybrid discharges with D-fuelling and a mixture of D+N fuelling. The contribution of fast particles (corresponding in average to ~15% reduction of the nominal confinement value) has been subtracted in order to identify the thermal part of the confinement. With pure deuterium fuelling, the standard H-mode behaviour is observed: at low D-fuelling (Pulse No: 68505) the hybrid discharges achieve $H98_{(y,2)}^{*} \geq 1$ while high D-fuelling is accompanied by a reduction of the global confinement: ~10% losses with $\Phi_D = 5\times10^{22}$ e/s (Pulse No: 68515) and ~20% losses with $\Phi_D = 9\times10^{22}$ e/s (Pulse No: 68739) without significant increase of the radiated fraction. Although N-seeding also reduces the global energy confinement, it enables to reach higher radiated fraction than with D-fuelling alone. The degradation of global confinement associated with the type-III ELM regime is about 10% compared to the reference hybrid high D-fuelling discharge (Pulse No: 68515), which uses the same D-fuelling: $\Phi_D = 5\times10^{22}$ e/s. The observed loss of energy confinement has to be balanced with the reduction of the peak heat flux by a factor of 4: $\langle Q_{target}^{OSP} \rangle = 1.7$MW m^{-2} is measured during the reference high D-fuelling hybrid regime Pulse No: 68515 and $\langle Q_{target}^{OSP} \rangle = 0.4$MW m^{-2} during the type-III ELM hybrid regime Pulse No: 68532.

Figure 15 shows that the confinement is stabilized or even slightly improved when the radiative fraction is high ($H98^{*}_{(y,2)}$ lies between 0.75 and 0.83 when $P^{rad}/P^{tot} \geq 0.4$). A first series of possible candidates responsible for the stabilization of the $H98^{*}_{(y,2)}$ factor observed in the newly developed type-III ELM regime could be:

- the quantity of nitrogen already present in the machine (trapped and released from the previous discharges),
- the amplitude of the N fuelling rate which are different,
- different MHD properties (but the similar MHD characteristics observed in this series of discharges seems to discredit this cause).
- the possible sensitivity of the nitrogen transport (penetration and dilution into the main plasma) to the plasma edge characteristics (position, amplitude and stiffness of the pedestal, temperature and density gradients).

This is illustrated in figures 16 and 17 when comparing Pulse No: 68746 (Pre-programmed and lower N fuelling rate) with Pulse No: 68532 (Feedback and highest N fuelling rate). Using similar and constant D fuelling rate, the latter has about 10% better core performances.

The pulse with the lower N fuelling rate at the beginning of the plateau (Pulse No: 68746, which has also lower N^{5+} brightness as shown in figure 16b) ends up with a mixed phase of small type-I and type-III ELMs phases while the pulse with the highest N fuelling rate at the beginning ends up with a pure Type-III ELM behavior, a high Z_{eff} (~3) and $P^{rad}/P^{tot} > 40\%$. In the plasma core, the nitrogen concentration (measured with the core Charge Exchange Recombination Spectroscopy system [33, 34]) in the high N-fuelling case (N^{7+}/n_e~2%) is about twice the value measured in the moderate and constant N-fuelling case (N^{7+}/n_e ~1%) – as shown in figure 17a.

In the plasma core, impurity seeding does not systematically cool the plasma because of radiation. In contrast to the plasma edge, the plasma core contains low-Z impurities that are mostly completely striped and the radiated power becomes negligible compared to the convected-conducted power. In this region, the increase of impurity concentration (and Z_{eff}) can have various effects on the plasma properties. It can play on the plasma resistivity (μ impurity concentration), on the power absorption (α density) and also on the transport and confinement properties (driven by instabilities and anomalous transport). Figure 16b shows that the central electron temperature does increase when the N concentration (measured with the core Charge Exchange Recombination Spectroscopy system [33], [34] and plotted in figure 17a) and Z_{eff} increase: $T_e^{central} = 3200 \rightarrow 3700$ eV whereas $Z_{eff} = 2.5 \rightarrow 3$. One possible mechanism responsible for the central temperature increase in impurity seeded plasmas is the suppression of Ion Temperature Gradient (ITG) instability through ion effective charge increase [35]. A complete and dedicated transport (using integrated modeling codes like TRANSP or CRONOS [36]) and stability analysis (using stability code like KINEZERO [37]) is required to validate this hypothesis and check if the increase of the central temperature when Z_{eff} is higher could be responsible for the relative improvement of the confinement energy in Pulse No: 68532 where $H98^*_{(y,2)} \sim 0.83$ compared to Pulse No: 68746 where $H98^*_{(y,2)} \sim 0.77$.

CONCLUSIONS

The type III ELM regime has been achieved during hybrid H-mode operation in the JET tokamak (with $I_p = 1.7$MA, $B_t = 1.7$T, $n_e \sim 0.95 \cdot n_{Gr}$ and $\beta_N \sim 2.6$) using both deuterium and nitrogen fuelling (this regime is triggered here when the inter-ELM radiated fraction reach approximately 40%). The newly developed integrated hybrid type III ELM scenario shows acceptable edge plasma conditions for the wall and moderate MHD activity including mild n=1 sawteeth precursors and residual MHD island (4/3NTM), which means q_{min} is close to unity. The core q-profile of the integrated hybrid type III ELM is very similar to the q-profile of the reference hybrid type I ELM scenario, indicating that it is also compatible with high β_N operation with minimized impact of sawteeth on stability (that leads for example to lower probability to trigger 3/2 and 2/1NTMs). The target temperature on the outer strike point is significantly reduced and the peak heat flux is reduced by about a factor of

4 compared to the reference hybrid type I ELM scenario. The carbon erosion is also reduced and partially replaced by nitrogen chemical activity. The counterpart effect of the improvement of the edge conditions (concerning the plasma-wall interaction issue) is a reduction of ~ 20% of the total plasma energy confinement ($H98^{*}_{(y,2)}$~0.83 is obtained during the hybrid type III ELM scenario). This situation is identical to the case of the "standard H mode" with large sawteeth: the transition from type-I to type-III ELMs also causes ~ 20% degradation of the energy confinement time. A marginal but interesting plasma core effect, depicted by the relative increase of the central plasma temperature when the effective charge of the plasma increases, has been observed in the type III ELM regime. This phenomenon is marginal for the plasma energy confinement but becomes essential for the comprehension of the core plasma behavior when impurity seeding is applied.

Due to the low confinement achieved during the hybrid type III ELM regime ($H98^{*}_{(y,2)}$~0.83), the scenario proposed in this paper is presently not favorable for ITER operation with the nominal fusion performance (pulsed operation with Q=10 and $H98^{*}_{(y,2)}$=1). A second physics objective of ITER is to meet Q = 5 in steady state plasma operation. If the confinement time of future ITER hybrid discharges (presently foreseen at low plasma current I_p ~ 14MA) is high enough to allow type III ELM operation with acceptable fusion performance (Q>5), then the experimental procedure described here can be envisaged to control the edge plasma conditions and get sustainable heat load (compatible with the ITER walls) without modifying the core q profile, and thus the high β_N capability of the hybrid scenario (optimized for current drive sources and non-inductive current bootstrap).

In addition to the problem of confinement, the relatively high impurity content and the extrapolation to ITER remain important issues to demonstrate the viability of the hybrid type III ELM scenario as an integrated scenario for ITER. Promising techniques are currently used or under development to suppress the impurity accumulation, for example injection of radio frequency power [38, 39, 40] or high densities operation with lower plasma core pollution [41]. A step before ITER operation, the newly developed hybrid type III ELM scenario can also be use in JET for high b_N operation with the future ITER-like wall (with tungsten and beryllium inertial tiles, e.g. with no actively cooled system). Better understanding of the recycling properties of nitrogen, use of the real-time control, maximization of confinement as observed in ASDEX Upgrade [42] and impurity decontamination techniques will be essential to improve the performances and the reliability of the scenario.

ACKNOWLEDGMENTS:

This work, supported by the European Communities under the contract of Association between EURATOM and CEA, was carried out within the framework of the European Fusion Development Agreement. The views and opinions expressed herein do not necessarily reflect those of the European Commission

REFERENCES:

[1]. ITER physics basis, 1999 *Nucl. Fusion* **39** No 12

[2]. Sips A.C.C, *et al* 2002 *Plasma Phys. Control. Fusion* **44** B69-B83
[3]. Luce T C, *et al* 2003 *Nucl. Fusion* **43** 321-329
[4]. E. Joffrin, *et al* 2007 *Nucl. Fusion* **647** 1664-1672
[5]. E. Joffrin, *et al* and JET-EFDA Contributors to the Work Programme 2005 *Nucl. Fusion* **45** 626-634
[6]. Matthews G F, *et al* and ITER-like wall team. Development of divertor Tungsten coatings for the ITER-like wall project 2008 *18th PSI conference* Toledo, Spain
[7]. Riccardo V. on behalf of the ITER-like wall Engineering Design and Manufacturing Team. ´Engineering challenges of the JET ITER-like wall[a]. *18th PSI conference*, Toledo, Spain (2008)
[8]. Rapp J, *et al* 2005 *Nucl. Mater.* **337-339** (2005) 826-830.
[9]. Monier-Garbet *et al* and JET-EFDA contributors 2005 Nucl. Fusion **45** 1404-1410
[10]. Saibene G, *et al* 1999 Nucl. Fusion **39** 1133-1156
[11]. Chankin A V and Saibene G 1999 *Plasma Phys. and Control. Fusion* **41**†913-930
[12]. Sartori R,*et al* 2004 *Plasma Phys. and Control. Fusion* **46** 723-750
[13]. E. Joffrin, *et al* and contributors to the JET EFDA Programme. 2003 *Plasma Phys. and Control. Fusion* **45** A367-A383
[14]. Petrie T W, *et al* and DIII-D team. 2007 *J. Nucl. Mater.* **363-365** 416-420
[15]. Koslowski H R, Nave M F, Alper B, Perez von Thun C, Pinches S, Sauter O, Sharapov S E. *18-22 June 2001 28th EPS conference*, Funchal, ECA Vol. 25A 965-968
[16]. Chang Z and Callen J D, 1990 *Nucl. Fusion* **2** 219
[17]. Andrew Y, Hawkes N C, Crombe K 2006 *Rev. Sci. Intrum.* **77** 10E913
[18]. Gauthier E, Andrew P, Arnoux G, Corre Y, Roche H and JET-EFDA Contributors 2007 *J. Nucl. Mater.* **363-365** 1026-1031
[19]. Herrmann A, Junker W, Gunther K, Bosch S, Kaufmann M, Neuhauser J, Pautasso G, Richter Th and Schneider R 1995 *Plasma Phys. Control. Fusion* **37** 17-29
[20]. Beurskens M.N.A, *et al* 2008 *Nucl. Fusion* **48** N∞9
[21]. Arnoux G, *et al* 2008 *18th PSI conference*, Toledo, Spain
[22]. Rapp J, Eich T, von Hellermann M, Herrmann A, Ingesson L C, Jachmich S, Matthews G F, Philipps V, Saibene G and contributor to the EFDA-JET Workprogramme., *Plasma Phys. And Control Fusion* **44** (2002) 639-652
[23]. Salzmann H, Bundgaard J, Gadd A, Gowers C, Hansen K B, Hirsch K, Nielsen P, Reed K, Schrödter C, and Weisberg K 1988 *Rev. Sci. Instrum.* **59** No 8 1451-1456 "The LIDAR Thomson scattering diagnostic on JET (invited)"
[24]. Loarte A, Saibene G and Sartori R 2004 *Phys. of Plasma.* **11** No 5, Part 2, 2668-2678
[25]. Pasqualotto R, Nielsen P, Gowers C, Beurskens M, Kempenaars M, Carlstrom M, Johnson D. 2004 *Rev. Sci. Instrum.* **75** 3891
[26]. Gauthier E, *et al Fusion Engineering and Design* (2007) **82** 1335-1340
[27]. Pitts R.A., *et al* 2005 *J. Nucl. Mater.* **337-339** 146-153

[28]. Stamp M.F., Erents S.K., Fundamenski W., Matthews G.F., Monk R.D. 2001 *J. Nucl. Mater.* **290-293** 321-325

[29]. Brezinsek S., *et al* and JET-EFDA contributors 2005 *J. Nucl. Mater* **337-339** 1058-1063

[30]. Brezinsek S, *et al* 2005 *32nd EPS conference*, Tarragona, Spain

[31]. Tabarés F L, Rohde V and the ASDEX Upgrade Team 2004 *Plasma Phys. Control. Fusion* **46** 381-395

[32]. Esser H.G, Kreter A, Philipps V, Widdowson A M, Coad J P, Stamp M. 2008 *18th PSI conference* Toledo, Spain

[33]. Negus C.R, Giroud C, Meigs A G, Zastrow K-D, Hillis D L 2006 *Review of Scientific Instruments* **77** 10F102

[34]. Giroud C, *et al* 2008 *High Temperature Plasma Diagnostic conference*, Albuquerque, New Mexico

[35]. Tokar M.Z. 2003 *Plasma Phys. Control. Fusion* **45** 1323-1332

[36]. Basiuk V, *et al* 2003 *Nucl. Fusion* **43** 822-30.

[37]. Bourdelle C, Garbet X, Hoang T G, Ongena J and Budny R V. 2002 *Nuclear Fusion* **42** 892-902

[38]. Dux R, Giroud C, Neu R, Peeters A G, Stober J, Zastrow K D. 2003 *Journal of Nuclear Materials*, **313-316** 1150-1155

[39]. Carraro L, *et al* 2007 *34nd EPS conference*, Warsaw, Poland

[40]. Nave M.F.F, *et al Nucl. Fusion* **43** 1204-1213

[41]. Rapp J, *et al* 2008 *18th PSI conference* Toledo, Spain

[42]. Sips A.C.C.C. et al. 2002 *Plasma Phys. and Control. Fusion* **44** A151

Pulse No:	68505	68507	68508	68509	68510	68514	68515	68516	68739	68746	68532
Φ_D	0.6e22	0.6e22	0.6e22	0.6e22	0.6e22	2e22	5e22	7e22	9e22	5e22	5e22
Φ_N	0	2e21	7.5e21	1.6e22	2.1e22	0	0	0	0	2.7e21	FB
$\langle f_{ELM} \rangle$	50	50	50	40	40	65	60	60	65	> 100	500
type	I	I	I	I	I	I	I	I	Mix	Mix	III
$\langle P^{tot} \rangle$	15	15.5	15.5	16	16	16.5	17	18	19	19.5	19.5

Table 1. Summarize of the D and N fuelling scans: fuelling rate (e/s), averaged ELM frequency (Hz), ELM type and averaged total injected power (MW). The last two columns show discharges discussed latter on in the paper (see chapter 5), #68532 is the reference hybrid type-III ELM.

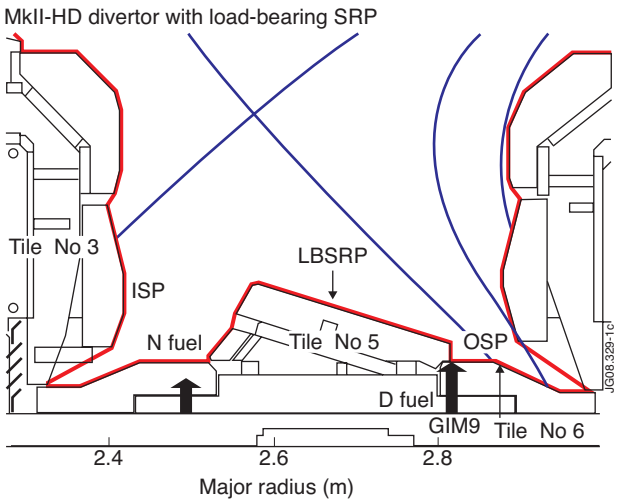

Figure 1: High triangularity magnetic configuration (δ = 0.44) and schematic of the MkIIHD divertor with load-bearing septum replacement plate (LBSRP). The N2 and D2 gas injection modules are located on the inner and outer sides, respectively. The last close surface shows the X-point and indicates the inner and outer strike points (ISP and OSP).

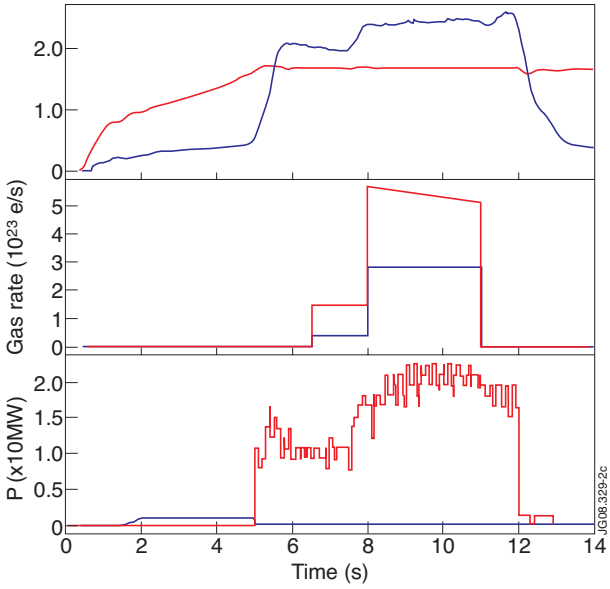

Figure 2: Plasma parameters and timing used to develop the hybrid type III ELM scenario. Pulde No: 68746 with pre-programmed N injection. (a) plasma current I_p and total normalized pressure β_N, (b) sub-divertor deuterium and nitrogen fuelling (given in electrons per second); gas introduction modules are presented in figure 1, (c) neutral beam and lower hybrid power.

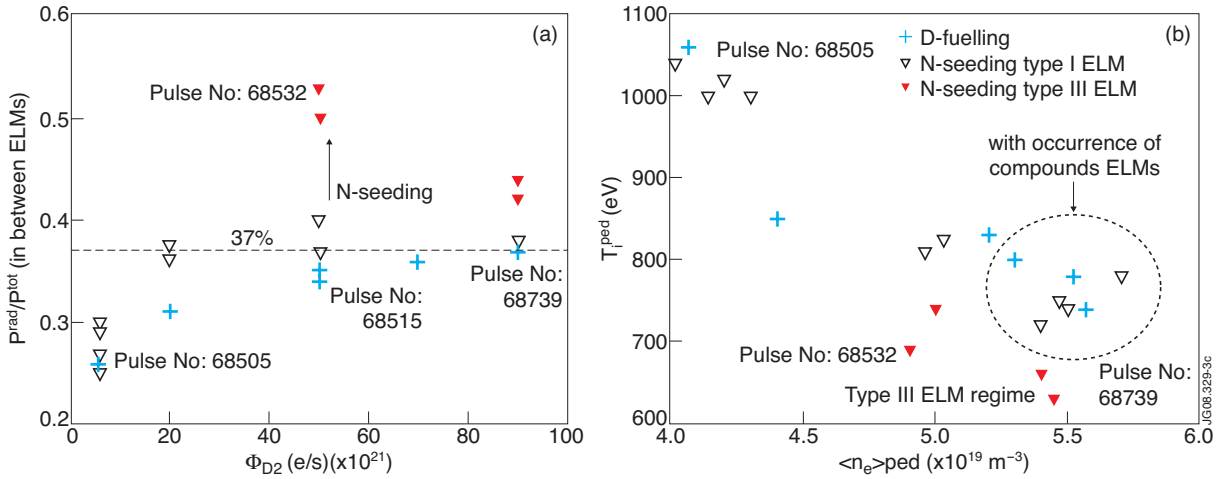

Figure 3: Set of JET discharges with various N_2 (HFS) and D_2 (LFS) fuelling rate. (a) Radiated fraction measured with the bolometers as a function of the deuterium fuelling rate (given in electron per second—the particle influx is obtained by using the atomic number and the charge factor, Z = 14 for N_2 and Z = 2 for D2). (b) Operational domain achieved with type I ELM and type III ELM regimes: T_i^{ped} measured with the edge Charge eXchange Recombination Spectroscopy (CXRS) diagnostic (averaged near the top of the pedestal) as a function of n_e^{ped} estimated with the interferometer diagnostic (vertical line average): Crosses represent discharges with D injection. Triangles represent discharges with D and N injection. Discharges where the type III ELM regime is achieved are filled up with black and type I ELM regime are filled up with white (including discharges with compounds ELMs).

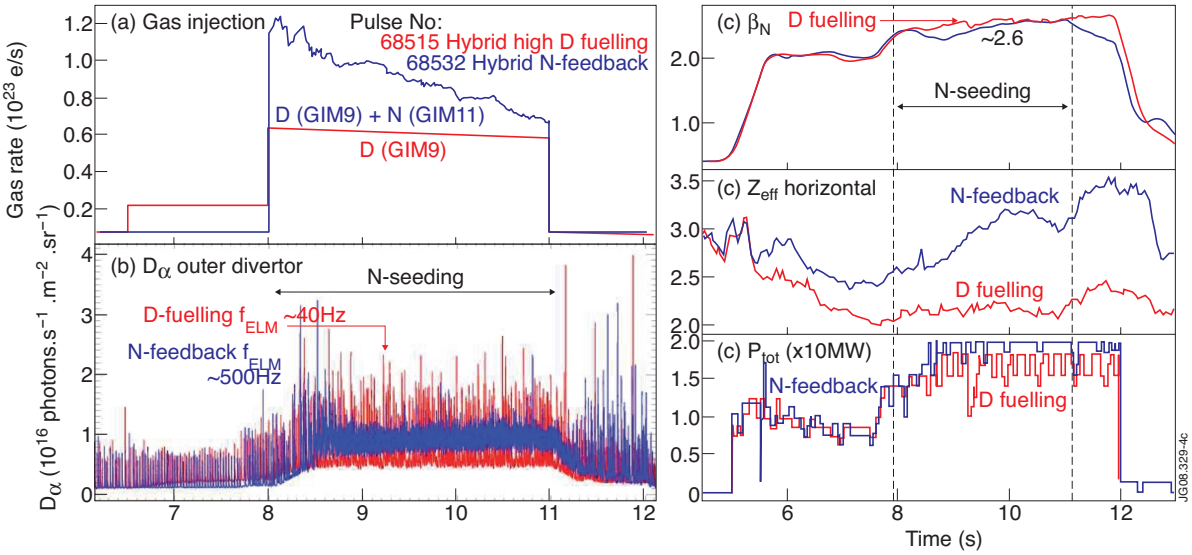

Figure 4: (a) Sub-divertor gas fuelling; gas introduction modules are presented in figure 1, (b) D_α signal in the outer divertor, (c) total normalized pressure β_N, (d) effective charge Z_{eff} estimated with the visible spectroscopy (chord in equatorial plan) and (e) neutral beam power for the reference type I (D fuelling) and type III (N-feedback) ELM regimes.

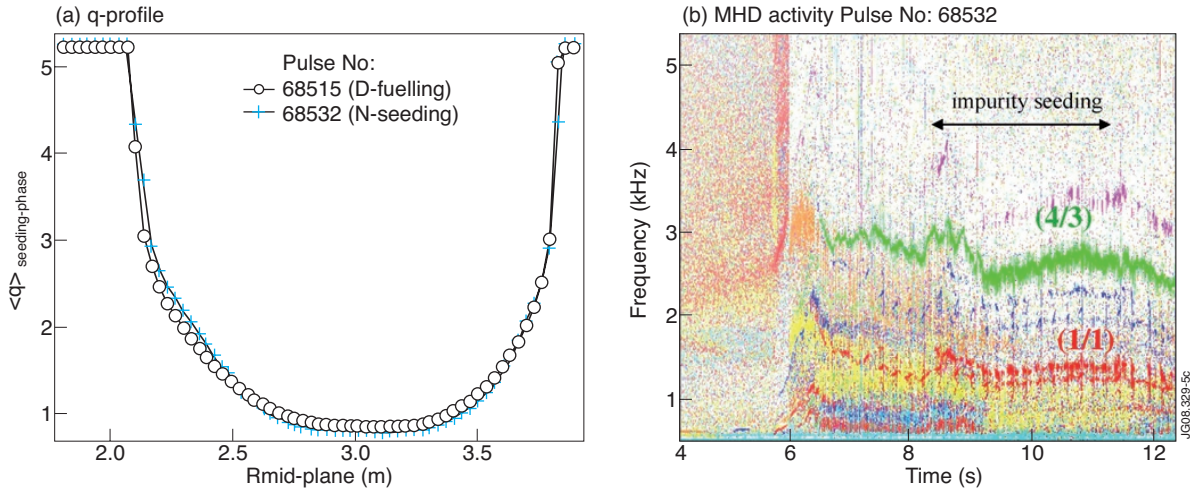

Figure 5: (a) Time average of q-profiles measured by the MSE system during the seeded phase t = [8–11s] for the pulse withDfuelling only (crosses) andD+Nfuelling (circles). (b) Spectrogram of one pick-up magnetic coil signal showing the MHD activity during Pulse No: 68532.

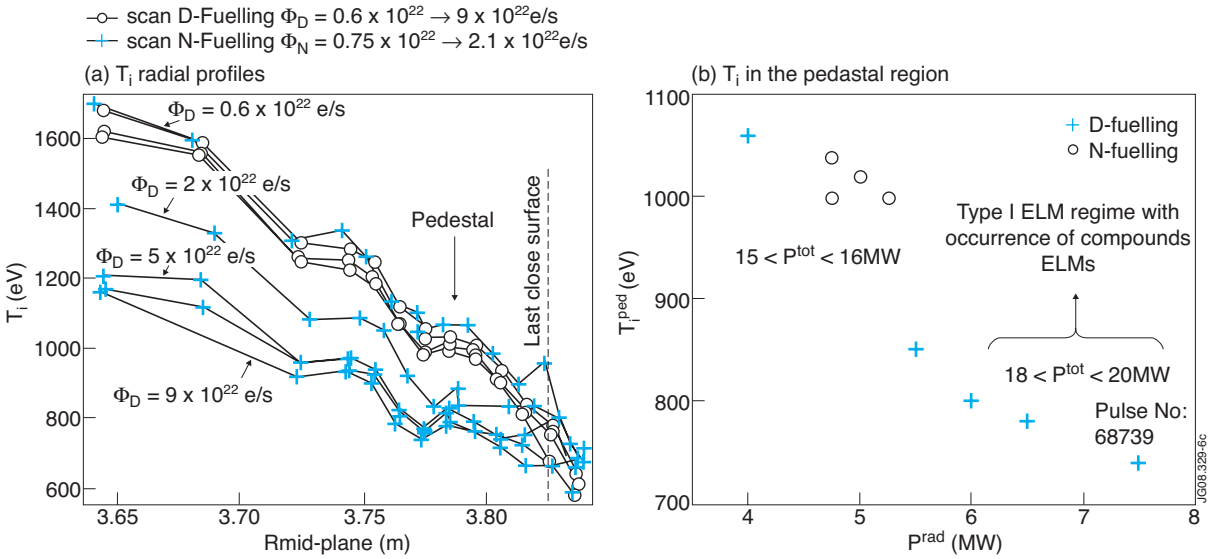

Figure 6: Ion temperature measured with the edge CXRS diagnostic. (a) T_i profiles as a function of the mid-plane position for a series of pulses with D (crosses) and N (circles) pre-programmed injection (equivalent electron influx). (b) Time average of T_i in the pedestal region as a function of the radiated power for the same series of pulses.

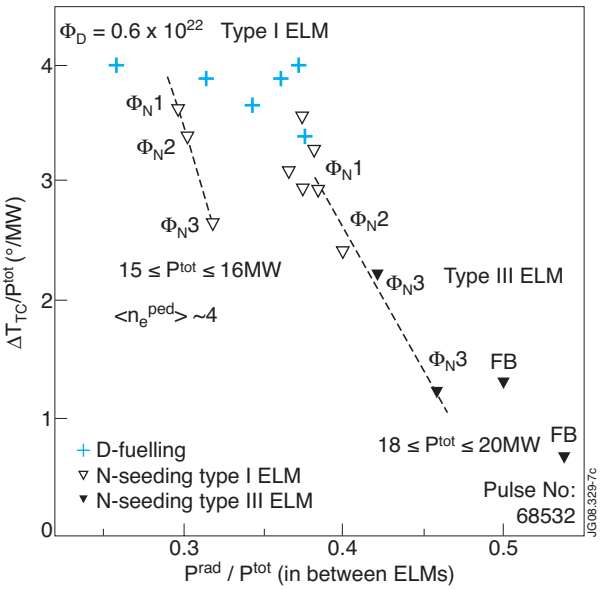

Figure 7: Difference of temperature measured in the bulk ΔT_{TC} (outer tile no 6) during the N-seeded phase divided by the total input power as a function of the radiated power fraction for a series of pulses with D (crosses) and D + N (triangles) injection: Φ^1_N = 0.7×10^{22} es^{-1}; Φ^2_N = 1.5×10^{22} es^{-1}; Φ^3_N = 2.2×10^{22} es^{-1}, FB represents the radiative feedback control (with variable Φ_N).

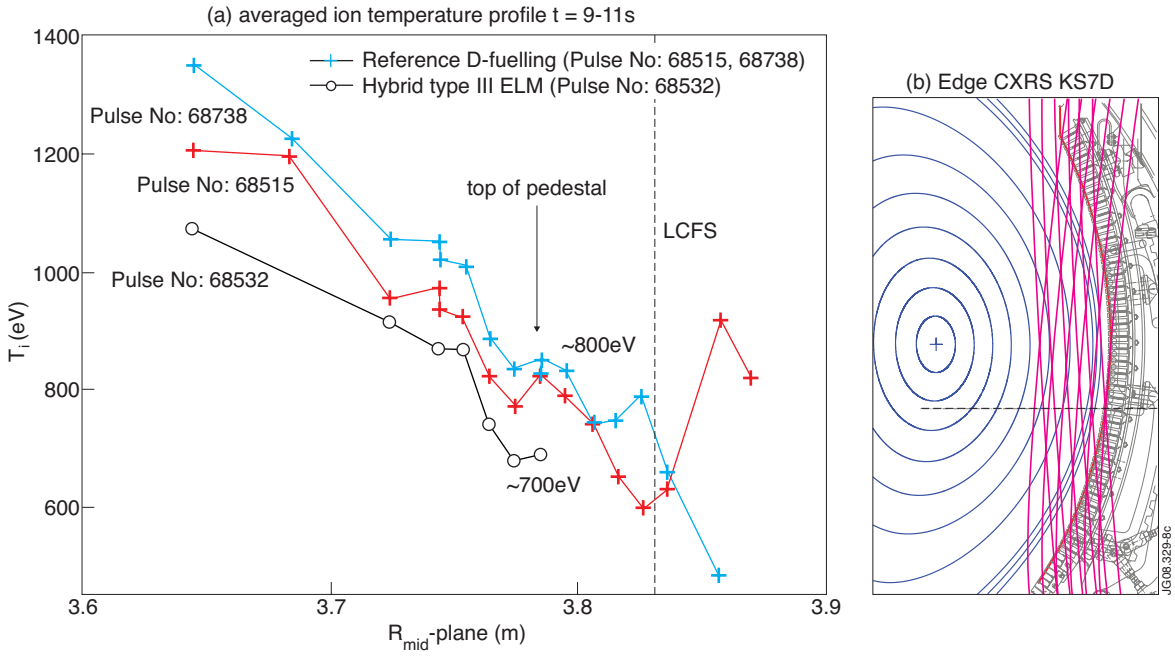

Figure 8: (a) Time average of the ion temperature profiles as measured with the edge charge exchange recombination spectroscopy (CXRS) diagnostic, averaged over t = [8–11s], for the reference hybrid high D fuelling (crosses: Pulse No's: 68515 and 68738) and the hybrid type III ELM (circles: Pulse No: 68532) discharges. (b) Lines of sight of the edge CXRS diagnostics in the JET poloidal section.

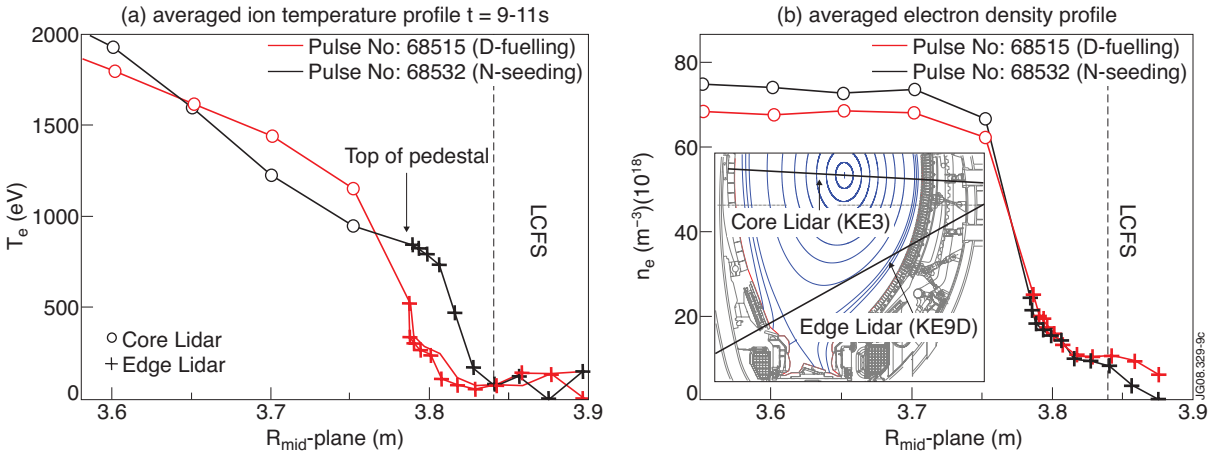

Figure 9: Electron (a) temperature and (b) density profiles such as measured with the core and edge LIDAR Thomson scattering diagnostics, time average over t = [9–11s]. The lines of sight for the edge and core LIDAR diagnostics in the JET poloidal section are also indicated.

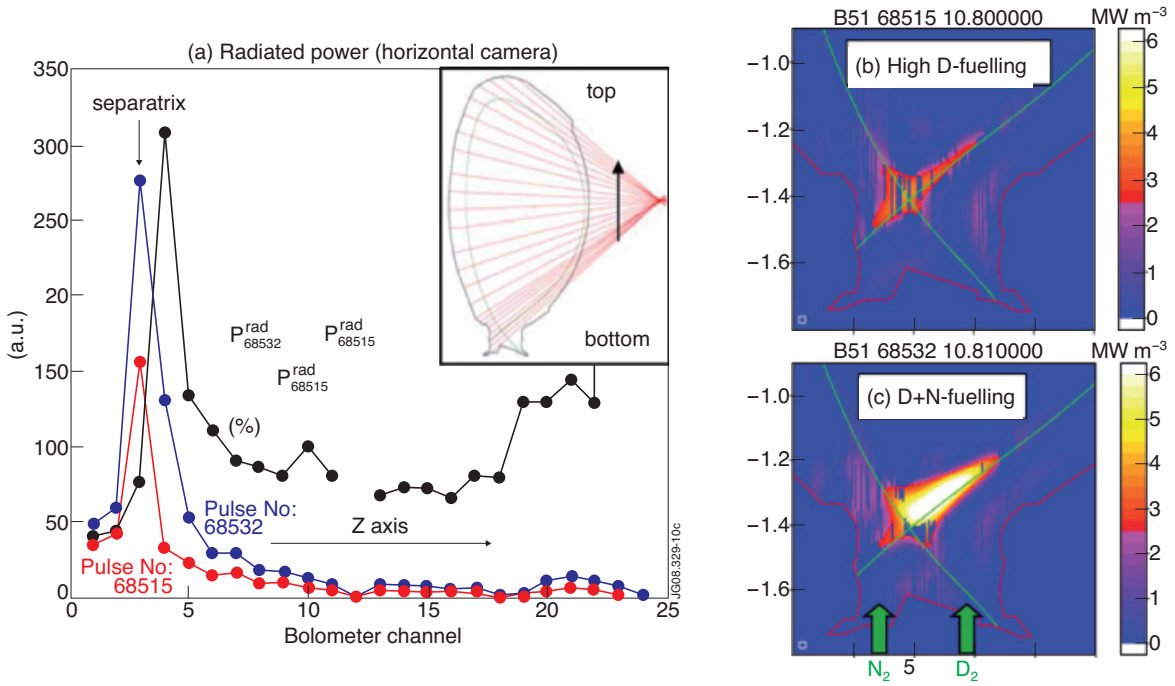

Figure 10: (a) Radiated power profile along the vertical axis taken in the inter-ELM phase, for the reference hybrid scenario (Pulse No: 68515) and hybrid type III ELM scenario (Pulse No: 68532). Radiated power modification due to N seeding in % (black curve). Tomographic reconstructions of Prad in the divertor: (b) reference hybrid and (c) hybrid type III ELM scenario with N seeding.

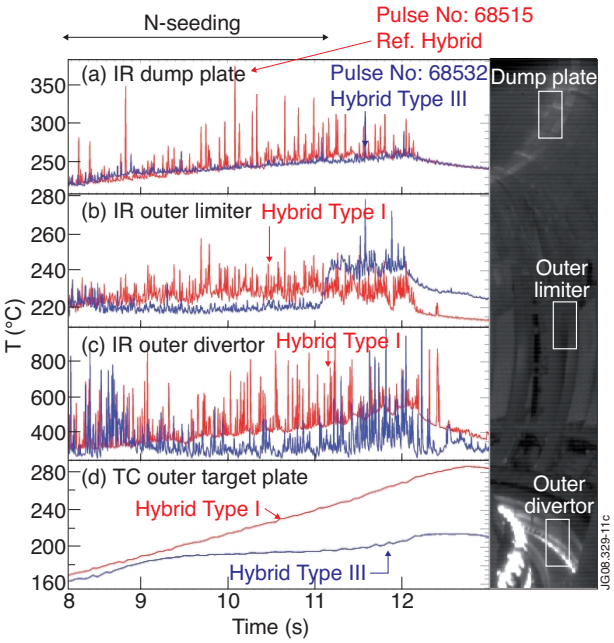

Figure 11. (a) Maximum surface temperature on the dump plate, (b) the outer limiter and (c) the outer divertor region. (d) Bulk temperature into the horizontal target plate (at 1cm deep) in the low-field side—below the OSP. N seeding is applied during t = 8–11s.

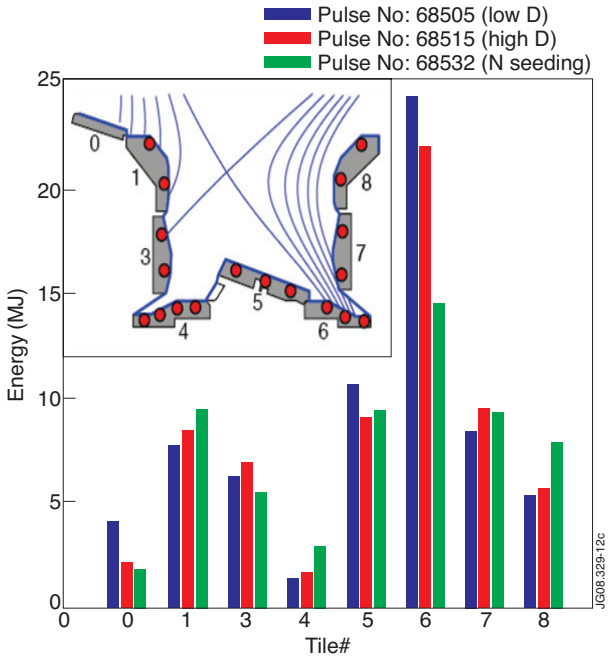

Figure 12. Energy distribution loaded in the divertor tiles (integrated over the all discharge) during reference and N-seeding pulses.

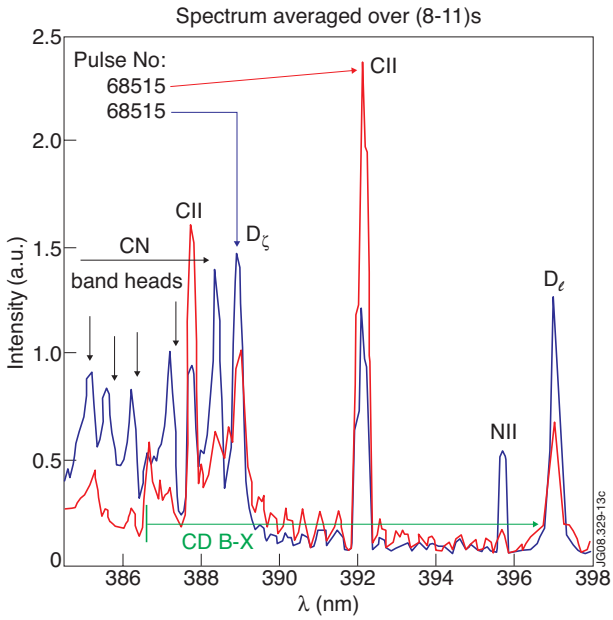

Figure 13. KT3A UV spectrum averaged over the N-seeding phase (therefore ELM and inter-ELM averaged) showing CN bands in Pulse No's: 68515 (reference) and 68532 (N-seeded).

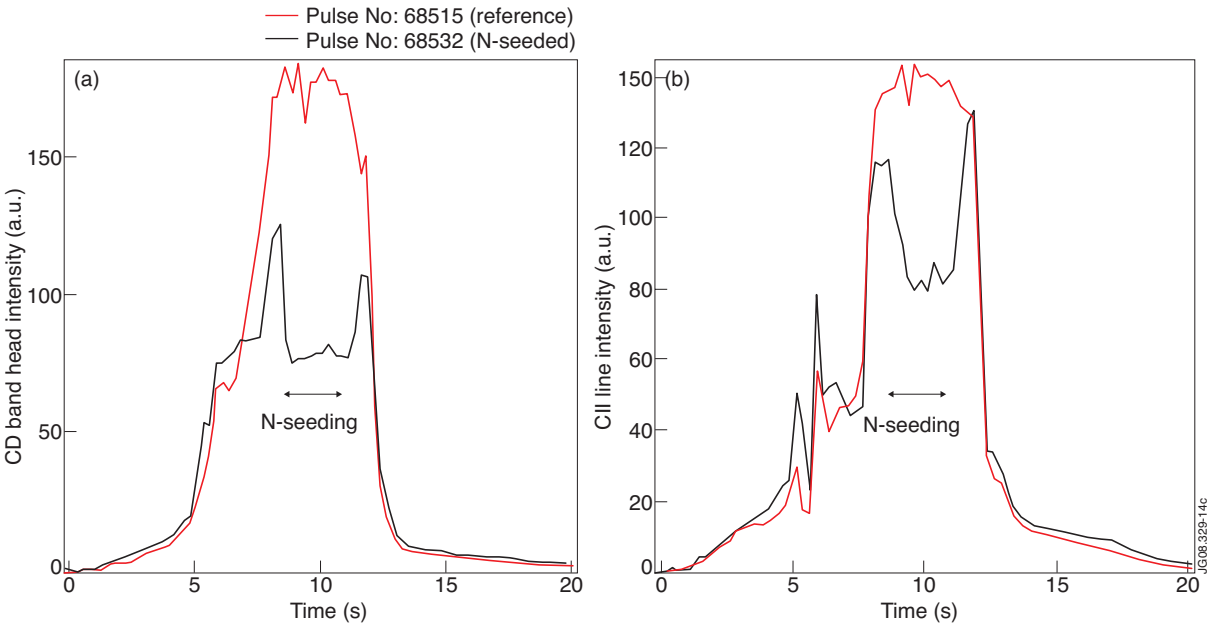

Figure 14: (a) Time evolution of the CD Ger¨o band (integrated over the range λ = 429.5–431nm) and (b) CII (λ = 426.7nm) line intensity during the reference (Pulse No: 68515) and type III ELM (Pulse No: 68532) hybrid discharges showing a reduction in CD and CII emission with N injection.

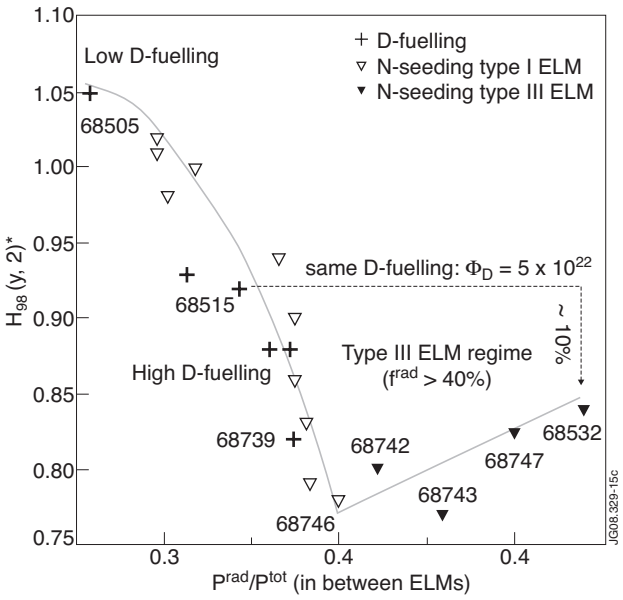

Figure 15: Thermal confinement enhancement factor $H98^*_{(y,2)}$ versus the radiated fraction measured in between ELMs for a series of pulses with D fuelling only (crosses) and D+N fuelling (white and black triangles are associated with type I and III ELM regimes, respectively).

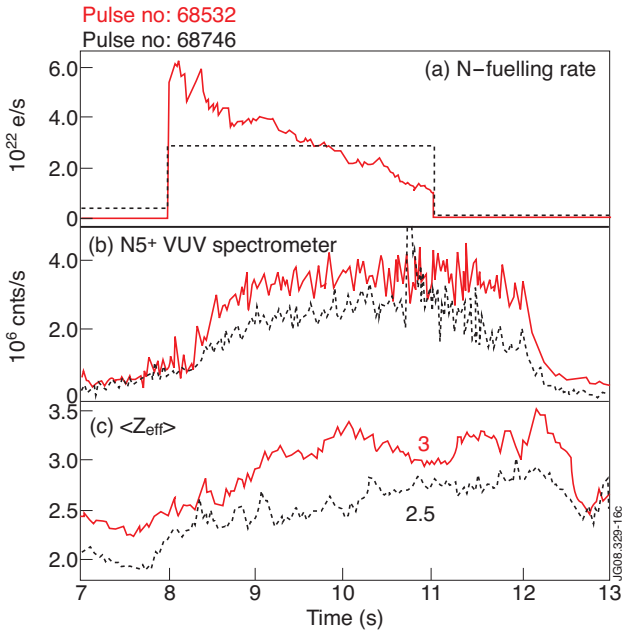

Figure 16: (a) N-fuelling rate (HFS). (b) N5+ radiation measured with the VUV spectrometer. (c) Z_{eff} measured during Pulse No's: 68532 and 68746.

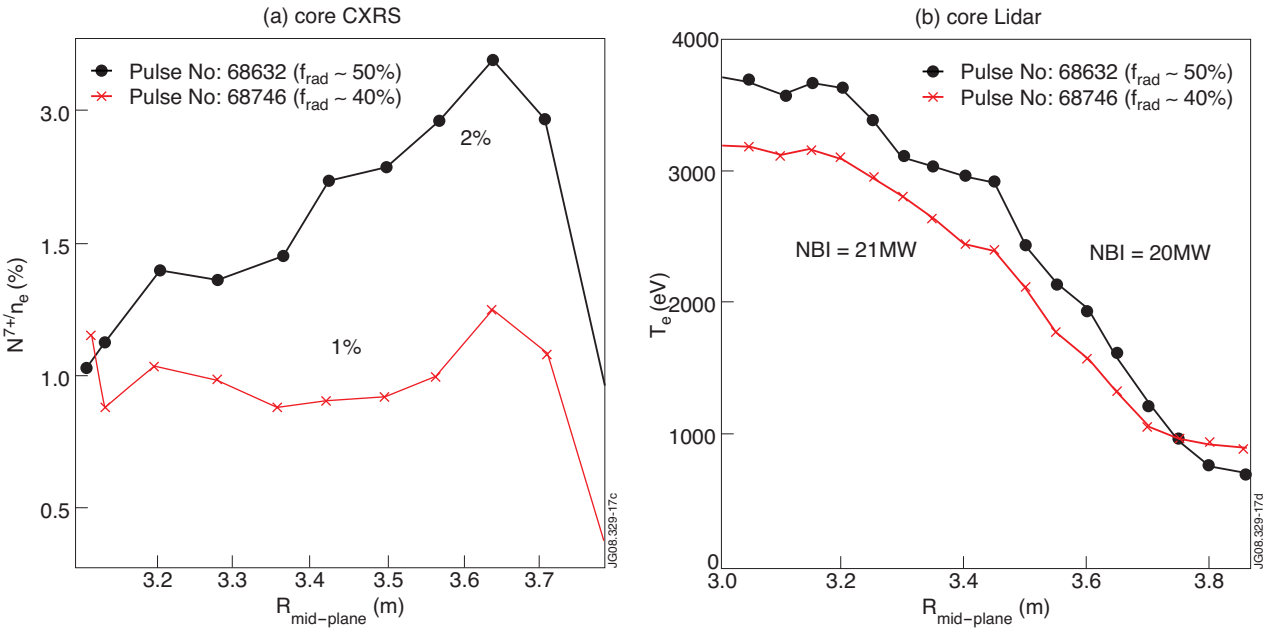

Figure 17: (a) N concentration and (b) electron temperature in the plasma core averaged over the seeding phase (t = 48–51s) measured during Pulse No's: 68532 (high start-up N-fuelling rate) and 68746 (moderate start-up N-fuelling rate).